Journal of Neurochemistry

JOURNAL OF NEUROCHEMISTRY | 2016

doi: 10.1111/jnc.13716

ORIGINAL ARTICLE

# Discovery of a fluorinated 4-oxo-quinoline derivative as a potential positron emission tomography radiotracer for imaging cannabinoid receptor type 2

Roger Slavik,* Adrienne Müller Herde,* Ahmed Haider,* Stefanie D. Krämer,* Markus Weber,† Roger Schibli,*,‡ Simon M. Ametamey* and Linjing Mu*,‡

*Institute of Pharmaceutical Sciences, ETH Zurich, Zurich, Switzerland

†Neuromuscular Diseases Unit/ALS Clinic, Kantonsspital St. Gallen, St. Gallen, Switzerland

‡Department of Nuclear Medicine, University Hospital Zurich, Zurich, Switzerland

**Abstract**

The cannabinoid receptor type 2 (CB2) is part of the endocannabinoid system and has gained growing attention in recent years because of its important role in neuroinflammatory/neurodegenerative diseases. Recently, we reported on a carbon-11 labeled 4-oxo-quinoline derivative, designated RS-016, as a promising radiotracer for imaging CB2 using PET. In this study, three novel fluorinated analogs of RS-016 were designed, synthesized, and pharmacologically evaluated. The results of our efforts led to the identification of *N*-(1-adamantyl)-1-(2-(2-fluoroethoxy)ethyl)-8-methoxy-4-oxo-1,4-dihydroquinoline-3-carboxamide (RS-126) as the most potent candidate for evaluation as a CB2 PET ligand. [$^{18}$F]RS-126 was obtained in ≥ 99% radiochemical purity with an average specific radioactivity of 98 GBq/μmol at the end of the radiosynthesis. [$^{18}$F]RS-126 showed a $\log D_{7.4}$ value of 1.99 and is stable *in vitro* in rat and human plasma over 120 min, whereas 55% intact parent compound was found *in vivo* in rat blood plasma at 10 min post injection. *In vitro* autoradiographic studies with CB2-positive rat spleen tissue revealed high and blockable binding which was confirmed in *in vivo* displacement experiments with rats by dynamic PET imaging. *Ex vivo* biodistribution studies confirmed accumulation of [$^{18}$F]RS-126 in rat spleen with a specificity of 79% under blocking conditions. The moderate elevated CB2 levels in LPS-treated mice brain did not permit the detection of CB2 by [$^{18}$F]RS-126 using PET imaging. In summary, [$^{18}$F]RS-126 demonstrated high specificity toward CB2 receptor *in vitro* and *in vivo* and is a promising radioligand for imaging CB2 receptor expression.

**Keywords:** biodistribution, CB2 ligands, fluorine-18 radiolabeling, *in vitro* autoradiography, neuroinflammation, positron emission tomography.

*J. Neurochem.* (2016) 10.1111/jnc.13716

Although the effects of cannabinoids have been known for centuries, the functional receptors (CB1 and CB2) were discovered only in the past decades through investigations on potential targets for cannabidiol and $\Delta^9$-tetrahydrocannabinol, the two pharmacologically most active ingredients of the hemp plant *Cannabis sativa* (Matsuda *et al.* 1990; Munro *et al.* 1993). Both CB1 and CB2 belong to the class A (rhodopsin family) G protein-coupled receptor family. The CB1 receptors are abundantly expressed in the central nervous system (CNS) and their function has been thoroughly investigated. The CB2 receptors are found predominantly in cells of the immune system, e.g. in the spleen, thymus or peripheral blood mononuclear cells and have very low to undetectable expression levels in the CNS under basal conditions (Galiegue *et al.* 1995). Cannabinoid receptors have gained attention as potential therapeutic targets for

Received April 13, 2016; revised manuscript received June 8, 2016; accepted June 9, 2016.

Address correspondence and reprint requests to Dr Linjing Mu or Prof. Dr Simon M. Ametamey, Institute of Pharmaceutical Sciences, ETH Zurich, 8093 Zurich, Switzerland. E-mails: linjing.mu@usz.ch, simon.ametamey@pharma.ethz.ch

*Abbreviations used*: CB2, cannabinoid receptor type 2; DAST, diethylaminosulfur trifluoride; HBTU, 2-(1H-benzotriazol-1-yl)-1,1,3,3-tetramethyluronium hexafluorophosphate; HRMS, high-resolution mass spectrometry; PET, positron emission tomography; TSPO, translocator protein.

 

the treatment of neurodegenerative diseases, cancer, obesity, inflammatory bowel disease, and pain (Di Marzo 2009). CB1 agonists and antagonists are medically used to enhance or reduce appetite, relief pain, avoid vomiting and muscle spasticity, a major limitation for the therapeutic development of compounds that directly activate CB1 receptors is unwanted psychotropic effects (Pertwee 2009; Volkow *et al.* 2014). Because of these undesirable effects, growing attention is being paid to the second cannabinoid receptor CB2. The high expression of CB2 receptor in cells and tissue of the immune system as well as the enhancement of its expression following inflammatory insults (Wright *et al.* 2005; Mukhopadhyay *et al.* 2006), suggests that CB2 receptor selective ligands might be effective in modulating inflammation. Initial studies revealed that activation of CB2 receptor reduced the production of pro-inflammatory molecules in a number of murine and human cell types *in vitro* (Merighi *et al.* 2012). Selective CB2 ligands have the potential to be used to treat pain, inflammation, osteoporosis, CB2-expressing malignant gliomas, tumors of immune origin, and various immunological disorders. CB2 activation may also produce analgesic effects without the CNS-mediated side effects encountered with CB1 receptor agonists/antagonists.

Positron emission tomography (PET) is a non-invasive biomedical imaging technique that enables quantification and visualization of biochemical and physiological processes by monitoring the time-dependent distribution of trace amount of molecules labeled with positron-emitting isotopes. PET imaging can provide information about receptor localization and density and has proven to be a powerful technique in neurological research (Halldin *et al.* 2001; Ametamey *et al.* 2008; Honer *et al.* 2014; Piel *et al.* 2014). The development of radioligands for non-invasive PET imaging of molecular targets in the central and peripheral nervous systems is a demanding task. This is particularly true for the imaging of neuroinflammation and neurodegeneration. Historically, nearly all neuroinflammation PET radiotracer research was related with the 18-kDa translocator protein (TSPO, formerly called peripheral benzodiazepine receptor). Despite the great efforts that have been made in the development of TSPO radioligands (Boutin *et al.* 2007; Endres *et al.* 2009; Van Camp *et al.* 2010; Damont *et al.* 2015; Vicidomini *et al.* 2015), their use in PET imaging of neuroinflammation remains challenging. TSPO radioligands exhibit a high non-specific binding, have complex kinetics and variable concentrations in plasma-free fractions across human clinical cohorts (Chauveau *et al.* 2008; Owen and Matthews 2011; Turkheimer *et al.* 2015). The heterogeneous TSPO distribution in brain tissue and polymorphisms of the TSPO gene even hampers radiotracer affinity. Development of a PET radiotracer that binds to a different target that is enhanced in neuroinflammation is an attractive alternative. One such alternative to TSPO is CB2. CB2 expression in microglia is up-regulated during activation. Neuroprotective effects of CB2 agonists are associated with suppression of microglia activation *via* inhibiting the release of neurotoxic factors and by decreasing neuronal cell damage in cell or tissue culture models (Eljaschewitsch *et al.* 2006). Increased expression of CB2 under neuroinflammatory conditions was found in human brain (Benito *et al.* 2008). Prominent CB2 up-regulation was reported in brain tissues affected by multiple sclerosis, amyotrophic lateral sclerosis, Down syndrome, and Alzheimer's disease (Benito *et al.* 2007; Shoemaker *et al.* 2007; Solas *et al.* 2013). CB2-specific radiotracer can be used as a biomarker of neuroinflammation in the early preclinical stages of Alzheimer's disease, when no significant neuronal loss has yet developed (Savonenko *et al.* 2015). A number of PET radioligands have been evaluated, but most of the ligands have been plagued with either high non-specific binding, low affinity and selectivity, rapid metabolism, or inappropriate pharmacokinetics (Evens *et al.* 2008, 2009, 2012; Horti *et al.* 2010; Vandeputte *et al.* 2011; Ruhl *et al.* 2012; Turkman *et al.* 2012; Gao *et al.* 2014). Recently, we reported a novel carbon-11 radiolabeled tracer [$^{11}$C]RS-016 for imaging CB2 (Slavik *et al.* 2015b). High binding to CB2 was observed in CB2-positive tissues (spleen) in rodents and postmortem amyotrophic lateral sclerosis patient spinal cord tissues in *in vitro* autoradiography experiments. Biodistribution data confirmed the high and specific uptake of [$^{11}$C]RS-016 in rat spleen. Drawback of this tracer is the short physical half-life (20 min) of carbon-11 that limits its application to only centers with an on-site cyclotron/radiochemistry facility. Compared to $^{11}$C, the longer physical half-life of $^{18}$F (110 min) allows for multiple PET scanning of several individuals from a single preparation, and permits also the distribution of the radiopharmaceutical to other PET imaging centers that lack a radiochemistry facility. The high percentage (96.7%) and relatively low energy (635 keV) of positron $\beta^+$ emission result in a low radiation dose to patients and high-resolution images.

Herein, we present the synthesis of three fluorinated analogs of RS-016 namely RS-030, RS-122, and RS-126 (Fig. 1), and their binding affinities toward CB2. The most potent candidate, RS-126, was radiolabeled with fluorine-18 and its potential as a CB2 PET ligand was evaluated both *in vitro* and *in vivo*.

## Materials and methods

### General

All reagents and solvents were purchased from Sigma-Aldrich Chemie GmbH (Steinheim am Albuch, Germany), Merck (Darmstadt, Germany), Acros Organics (Belgium), ABCR GmbH (Karlsruhe, Germany) or Fluka (Buchs, Switzerland). All chemicals were used as supplied without further purification. $^1$H and $^{13}$C NMR spectra were

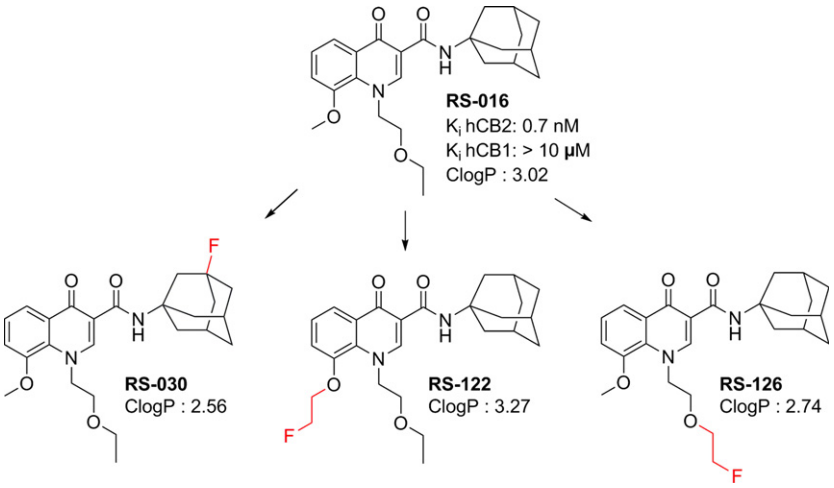


**Fig. 1** Three novel fluorinated RS-016 analogs.

obtained on a Bruker Avance FT-NMR spectrometer (400 MHz) (Bruker BioSpin AG, Fällanden, Switzerland). Chemical shifts are given in delta (δ) units, in ppm relative to tetramethylsilane (0 ppm). Multiplicities in the $^1$H-NMR spectra are described as: s = singlet, d = doublet, t = triplet, q = quartet, m = multiplet. Coupling constants (*J*) are reported in Hz. High-resolution mass spectrometry (HRMS) was performed on a Bruker's maXis (ESI-Qq-TOF-MS) spectrometer (Bruker Daltonik GmbH, Bremen, Germany) and are given in m/z. ClogP values were calculated using the CambridgeSoft Software ChemDraw 13.0 (PerkinElmer, Cambridge, MA, USA). For purification of the radiolabeled product, a semi-preparative Knauer Smartline 1050 HPLC system was used with an ACE C18-300 column (250 × 10 mm, 5 μm) with an isocratic solvent system 0.1% $H_3PO_4$ in $H_2O$ (60%) and $CH_3CN$ (40%) at a flow rate of 4 mL/min. For product analysis, an analytical Agilent 1100 series HPLC system (Agilent Technologies AG, Morges, Switzerland), equipped with UV multi-wavelength detector and a GabiStar radiodetector (Raytest) was used with an ACE C18-AR column (50 × 4.6 mm, 3 μm) with the following conditions: 0.1% trifluoroacetic acid in $H_2O$ (solvent A), $CH_3CN$ (solvent B); 0.0–3.0 min, 30% B; 3.1–13.0 min, 30–95% B; 13.1–15 min, 95% B at a flow rate of 1 mL/min.

## Chemistry

Synthesis of diethyl 2-(((2-methoxyphenyl)amino)methylene)malonate (1). A mixture of 2-anisidine (6.36 g, 51.6 mmol) and diethyl 2-(ethoxymethylene)malonate (11.17 g, 51.6 mmol) was stirred and heated in an oil bath at 110 °C for 1 h. After cooling to ambient temperature, the crude mixture was recrystallized from hexane (50 mL) to give 1 (13.36 g, 88%) as a yellowish solid. $^1$H NMR (400 MHz, $CDCl_3$): δ 11.12 (d, *J* = 14.0 Hz, 1H), 8.57 (d, *J* = 14.0 Hz, 1H), 7.25 (m, 1H), 7.12–7.08 (m, 1H), 7.00–6.97 (m, 1H), 6.95–6.92 (m, 1H), 4.33 (q, *J* = 7.1 Hz, 2H), 4.25 (q, *J* = 7.1 Hz, 2H), 3.94 (s, 3H), 1.38 (t, *J* = 7.1 Hz, 3H), 1.33 (t, *J* = 7.1 Hz, 3H). $^{13}$C NMR (100 MHz, $CDCl_3$): δ 168.5, 166.0, 150.4, 148.9, 128.8, 124.8, 121.2, 120.9, 119.1, 114.3, 111.2, 93.8, 60.3, 60.0, 55.9, 14.4, 14.3. HRMS calcd for $C_{15}H_{19}NNaO_5$ (M+Na) 316.1155, found 316.1164.

Synthesis of ethyl 8-methoxy-4-oxo-1,4-dihydroquinoline-3-carboxylate (2). Compound 1 (13.00 g, 44.3 mmol) was dissolved in diphenylether (70 mL). The reaction mixture was heated at 250 °C for 1 h. After cooling to ambient temperature, the mixture was filtered and the precipitates were washed with diphenylether (10 mL) and hexane (3 × 10 mL). After recrystallization from ethanol (150 mL), the precipitates were collected by filtration and dried under reduced pressure to give 2 (7.68 g, 70%) as a gray powder. $^1$H NMR (400 MHz, dimethylsulfoxide, DMSO): δ 11.92 (d, *J* = 4.2 Hz, 1H), 8.34 (d, *J* = 6.0 Hz, 1H), 7.70 (dd, *J* = 7.5 Hz, 1.9 Hz, $J_2$ = 7.5 Hz, 1H), 7.36–7.30 (m, 2H), 4.21 (q, *J* = 7.1 Hz, 2H), 4.00 (s, 3H), 1.27 (t, *J* = 7.1, 3H). $^{13}$C NMR (100 MHz, DMSO): δ 173.2, 164.2, 148.7, 144.0, 129.3, 128.1, 124.6, 116.7, 112.2, 110.0, 59.6, 56.3, 14.3. HRMS calcd for $C_{13}H_{13}NNaO_4$ (M+Na) 270.0737, found 270.0743.

Synthesis of ethyl 1-(2-ethoxyethyl)-8-methoxy-4-oxo-1,4-dihydroquinoline-3-carboxylate (3). To a solution of 2 (1.2 g, 4.85 mmol) in N, N-dimethylformamide (15 mL), potassium carbonate (1.34 g, 9.71 mmol) and 1-bromo-2-ethoxyethane (1.095 mL, 9.71 mmol) were added. The reaction mixture was heated at 90 °C for 4 h, cooled to RT (23–25°C) and then aq. HCl (0.2 M, 50 mL) was added. The mixture was extracted with $CH_2Cl_2$ (3 × 5 mL) and the combined organic layers dried over $MgSO_4$. Solvents were removed under reduced pressure and the residue was purified over silica gel using hexane/EtOAc (1 : 1) to give 3 (1.16 g, 75%) as a yellowish oil. $^1$H NMR (400 MHz, $CDCl_3$): δ 9.19 (s, 1H), 7.96 (dd, *J* = 8.3 Hz, 1.0 Hz, 1H), 7.49 (t, *J* = 8.3 Hz, 1H), 7.13 (d, *J* = 8.3 Hz, 1.0 Hz, 1H), 4.45 (q, *J* = 7.1 Hz, 2H), 4.40–4.38 (m, 2H), 4.08 (s, 3H), 3.85–3.83 (m, 2H), 3.57 (q, *J* = 7.0 Hz, 2H), 1.44 (t, *J* = 7.1 Hz, 3H), 1.20 (t, *J* = 7.0 Hz, 3H). $^{13}$C NMR (100 MHz, $CDCl_3$): δ 165.1, 164.1, 155.4, 150.8, 142.8, 126.9, 125.1, 115.2, 115.1, 109.8, 75.3, 69.6, 66.7, 61.5, 56.1, 15.1, 14.3. HRMS calcd for $C_{17}H_{22}NO_5$ 320.1492 (M+H), found 320.1488.

Synthesis of 1-(2-ethoxyethyl)-8-methoxy-4-oxo-1,4-dihydroquinoline-3-carboxylic acid (4). Aq. NaOH (10%, 100 mL) was added to 3 (1.5 g, 4.7 mmol). The reaction mixture was refluxed for 3 h. After cooling to ambient temperature, pH was adjusted to two using conc. HCl and the precipitates were filtered and washed with water (10 mL) and diethylether (10 mL). Recrystallization from EtOH (80 mL) gave 4 (1.16 g, 85%) as a yellowish solid. $^1$H NMR (400 MHz, $CDCl_3$): δ 14.95 (s, 1H), 8.18 (dd, *J* = 8.1 Hz, 1.4 Hz, 1H), 7.49 (t, *J* = 8.1 Hz, 1H), 7.29 (dd, *J* = 8.1 Hz, 1.4 Hz, 1H), 4.82 (t, *J* = 4.9 Hz, 2H), 4.00 (s, 3H), 3.76 (t, *J* = 4.9 Hz, 2H), 3.40

(q, $J$ = 7.0 Hz, 2H), 1.09 (t, $J$ = 7.0 Hz, 3H). $^{13}$C NMR (100 MHz, $CDCl_3$): δ 152.0, 126.5, 119.3, 115.5, 69.0, 66.8, 59.9, 56.5, 15.0. HRMS calcd for $C_{15}H_{18}NO_5$ (M+H) 292.1179, found 292.1175.

Synthesis of 1-(2-ethoxyethyl)-*N*-(3-hydroxyadamantan-1-yl)-8-methoxy-4-oxo-1,4-dihydroquinoline-3-carboxamide (RS-028). To a solution of 4 (63 mg, 0.216 mmol) in DMF (1.5 mL) was added di-isopropylethylamine (0.09 mL, 0.515 mmol). 2-(1H-benzotriazol-1-yl)-1,1,3,3-tetramethyluronium hexafluorophosphate (HBTU, 164 mg, 0.433 mmol) was added portion wise and the reaction mixture is stirred at 23–25°C for 30 min, then 3-hydroxy-1-aminoadamantane (36.2 mg, 0.216 mmol) was added. The reaction mixture was stirred at 23–25°C for 3 h. The mixture was diluted with ethyl acetate (EtOAc, 50 mL) and washed with water (3 × 15 mL), followed by diluted HCl (0.5M, 15 mL), water (15 mL) and then brine (20 mL). The organic solvent was evaporated under reduced pressure and the residue was purified with flash chromatography using $CH_2Cl_2$/MeOH (50 : 1 to 20 : 1) to give RS-028 (80 mg, 84%) as a white solid. $^1$H NMR (400 MHz, $CDCl_3$): δ 10.04 (s, 1H), 8.64 (s, 1H), 8.16 (dd, $J$ = 8.1 Hz, 1.4 Hz, 1H), 7.39 (t, $J$ = 8.0 Hz, 1H), 7.19 (dd, $J$ = 8.1 Hz, 1.2 Hz, 1H), 4.74 (t, $J$ = 5.4 Hz, 2H), 3.97 (s, 3H), 3.75 (t, $J$ = 5.4 Hz, 2H), 3.42 (q, $J$ = 7.0 Hz, 2H), 2.31–2.04 (m, 9H), 1.78–1.62 (m, 5H), 1.42 (s, 1H), 1.11 (t, $J$ = 7.0 Hz, 3H). $^{13}$C NMR (100 MHz, $CDCl_3$): δ 150.9, 114.3, 69.5, 59.0, 56.3, 49.3, 44.2, 40.5, 35.1, 30.7. HRMS calcd for $C_{25}H_{33}N_2O_5$ 441.2384 (M+H), found 441.2382.

Synthesis of 1-(2-ethoxyethyl)-*N*-(3-fluoroadamantyl)-8-methoxy-4-oxo-1,4-dihydroquinoline-3-carboxamide (RS-030). To a −78 °C cold solution of 1-(2-ethoxyethyl)-*N*-(3-hydroxyadamantyl)-8-methoxy-4-oxo-1,4-dihydroquinoline-3-carboxamide (RS-028) (11 mg, 0.023 mmol) in $CH_2Cl_2$ (0.25 mL), diethylaminosulfur trifluoride (DAST, 6 μL, 0.045 mmol) was added. The mixture was allowed to warm to 23–25°C and stirred for 1 h. Ice water (5 mL) was added and the reaction was extracted with $CH_2Cl_2$ (3 × 2 mL), washed with brine, dried over $MgSO_4$ and solvents were removed under reduced pressure. Crude was purified over silica gel using $CH_2Cl_2$/MeOH (50 : 1) to give RS-030 (10 mg, 91%) as a white solid. $^1$H NMR (400 MHz, $CDCl_3$): δ 10.09 (s, 1H), 8.64 (s, 1H), 8.16 (dd, $J$ = 8.1 Hz, 1.4 Hz, 1H), 7.39 (t, $J$ = 8.1, 1H), 7.19 (dd, $J$ = 8.1 Hz, 1.2 Hz, 1H), 4.74 (t, $J$ = 5.3 Hz, 2H), 3.97 (s, 3H), 3.75 (t, $J$ = 5.3 Hz, 2H), 3.41 (q, $J$ = 7.0 Hz, 2H), 2.37 (d, $J$ = 5.3 Hz, 4H), 2.17–1.85 (m, 8H), 1.65–1.55 (m, 2H), 1.12 (t, $J$ = 7.0 Hz, 3H). $^{13}$C NMR (100 MHz, $CDCl_3$): δ 151.0, 125.3, 119.4, 114.3, 69.5, 66.8, 59.0, 56.4, 46.5, 41.9, 41.8, 40.4, 34.9, 31.1, 31.0, 15.0. HRMS calcd for $C_{25}H_{32}FN_2O_4$ (M+H) 443.2341, found 443.2340.

Synthesis of *N*-(1-adamantyl)-1-(2-ethoxyethyl)-8-hydroxy-4-oxo-1,4-dihydroquinoline-3-carboxamide (5). To a solution of RS-016 (202 mg, 0.476 mmol) in DMF (5 mL) was added lithium chloride (303 mg, 7.14 mmol). The reaction mixture was heated to reflux and stirred overnight. After cooling to ambient temperature, EtOAc (60 mL) was added and the mixture was washed with HCl (0.2 M, 3 × 10 mL) and brine (15 mL). The organic layer was dried over $MgSO_4$ and solvents were removed under reduced pressure. HPLC purification over a C18 column using 0.1% TFA in water and acetonitrile (30 : 70, v : v) gave the desired product 5 (37 mg, 20%) as a yellowish powder. $^1$H NMR (400 MHz, $CDCl_3$): δ 10.00 (s, 1H), 8.65 (s, 1H), 8.33 (br s, 1H), 8.14 (dd, $J$ = 7.1 Hz, 2.5 Hz, 1H), 7.35–7.29 (m, 2H), 4.75 (t, $J$ = 4.9 Hz, 2H), 4.00 (t, $J$ = 4.9 Hz, 2H), 3.61 (q, $J$ = 7.0 Hz, 2H), 2.14–2.09 (m, 3H), 1.78–1.67 (m, 12H), 1.18 (t, $J$ = 7.0 Hz, 3H). $^{13}$C NMR (100 MHz, $CDCl_3$): δ 149.11, 125.62, 123.36, 119.80, 69.37, 67.81, 55.34, 41.76, 36.53, 31.93, 29.70, 29.53, 29.36, 14.62. HRMS calcd for $C_{24}H_{31}N_2O_4$ (M+H) 411.2278, found 411.2281.

Synthesis of *N*-(1-adamantanyl)-1-(2-ethoxyethyl)-8-(2-fluoroethoxy)-4-oxo-1,4-dihydroquinoline-3-carboxamide (RS-122). To a solution of 5 (20 mg, 0.05 mmol) and cesium carbonate (24 mg, 0.075 mmol) in DMF (1 mL) was added 2-fluoroethyl 4-methylbenzenesulfonate (13 μL, 0.075 mmol). The reaction mixture was stirred at 23–25°C for 24 h. The mixture was diluted with aq. HCl (0.2 M, 30 mL) and extracted with $CH_2Cl_2$ (3 × 5 mL). The combined organic layers were washed with brine (20 mL) and dried over $MgSO_4$. Solvents were removed under reduced pressure and the residue was purified over silica gel using $CH_2Cl_2$/MeOH (100 : 1) to give RS-122 (18 mg, 79%) as a white solid. $^1$H NMR (400 MHz, $CDCl_3$): δ 9.88 (s, 1H), 8.68 (s, 1H), 8.21 (dd, $J$ = 8.0 Hz, 1.4 Hz, 1H), 7.37 (t, $J$ = 8.0 Hz, 1H), 7.15 (dd, $J$ = 8.0 Hz, 1.2 Hz, 1H), 4.90–4.88 (m, 1H), 4.78–4.76 (m, 3H), 4.40–4.38 (m, 1H), 4.33–4.31 (m, 1H), 3.78 (t, $J$ = 5.3 Hz, 2H), 3.41 (q, $J$ = 7.0 Hz, 2H), 2.19–2.11 (m, 9H), 1.77–1.68 (m, 6H), 1.10 (t, $J$ = 7.0 Hz, 3H). $^{13}$C NMR (100 MHz, $CDCl_3$): δ 151.2, 124.9, 120.1, 114.9, 82.0, 80.3, 69.5, 68.7, 68.5, 66.7, 58.9, 51.6, 41.8, 36.6, 29.6, 15.0. HRMS calcd for $C_{26}H_{34}FN_2O_4$ (M+H) 457.2497, found 457.2495.

Synthesis of 8-methoxy-4-oxo-1,4-dihydroquinoline-3-carboxylic acid (6). To 2 (2.00 g, 8.09 mmol) was added aq. NaOH (10%, 140 mL). The reaction mixture was heated to reflux and stirred for 3 h. The pH was adjusted to 2 using conc. HCl and the precipitates were filtered and washed with water (15 mL) and petroleum ether 60/90 (20 mL). The residue was dissolved in EtOH (150 mL) and heated to reflux and stirred for 30 min. The mixture was cooled down slowly; the precipitates were filtered and dried in vacuum to give 6 (1.67 g, 94%) as a slight gray powder. $^1$H NMR (400 MHz, DMSO): δ 15.32 (s, 1H), 12.99 (s, 1H), 8.57 (s, 1H), 7.83 (dd, $J$ = 8.0 Hz, 1.4 Hz, 1H), 7.55 (t, $J$ = 8.0 Hz, 1H), 7.49 (dd, $J$ = 8.0 Hz, 1.2 Hz, 1H), 4.06 (s, 3H). $^{13}$C NMR (100 MHz, $CDCl_3$): δ 178.2, 166.2, 149.0, 143.9, 126.4, 125.3, 116.0, 113.5, 107.9, 56.6. HRMS calcd for $C_{11}H_{10}NO_4$ (M+H) 220.0604, found 220.0600.

Synthesis of *N*-(1-adamantyl)-8-methoxy-4-oxo-1,4-dihydroquinoline-3-carboxamide (7). To a solution of 6 (220 mg, 1 mmol) in DMF (8 mL), di-isopropylethylamine (524 μL, 3.00 mmol) was added and the reaction mixture was stirred at 23–25°C for 30 min. HBTU (758 mg, 2.00 mmol) was added portion wise, followed by the addition of 1-aminoadamantane (180 mg, 1.20 mmol). The mixture was stirred at 23–25°C for 3 h, diluted with EtOAc (50 mL) and washed with water (3 × 15 mL), aq. HCl (0.5M, 15 mL), water (15 mL) and then brine (20 mL). EtOAc was evaporated under reduced pressure and the residue was purified with flash chromatography using hexane/EtOAc (2 : 1 to 1 : 4) to give 7 (330 mg, 94%) as a yellowish powder. $^1$H NMR (400 MHz, DMSO): δ 12.28 (d, $J$ = 4.3 Hz, 1H), 10.02 (s, 1H), 8.58 (d, $J$ = 4.3 Hz, 1H), 7.82 (dd, $J$ = 7.9 Hz, 1.4 Hz, 1H), 7.43 (t, $J$ = 7.9 Hz, 1H), 7.39 (dd, $J$ = 7.9 Hz, 1.4 Hz, 1H), 4.06 (s, 3H), 2.10 (s, 9H), 1.71 (s, 6H). $^{13}$C NMR (100 MHz, $CDCl_3$): δ 142.5, 124.7, 116.5, 112.0, 56.3, 50.4, 41.4, 36.0, 28.8. HRMS calcd for $C_{21}H_{25}N_2O_3$ 353.1860 (M+H), found 353.1854.

Synthesis of *N*-(1-adamantyl)-1-(2-(2-bromoethoxy)ethyl)-8-methoxy-4-oxo-1,4-dihydroquinoline-3-carboxamide (8). To a

stirred solution of 7 (100 mg, 0.284 mmol) in DMF (2 mL), cesium carbonate (137 mg, 0.422 mmol) and 1-bromo-2-(2-bromoethoxy) ethane (53 μL, 0.422 mmol) were added. The reaction mixture was heated at 90 °C under nitrogen for 3 h. After cooling to ambient temperature, the mixture was poured into ice water (50 mL) and extracted with $CH_2Cl_2$ (3 × 10 mL), washed with brine (15 mL) and dried over $MgSO_4$. Solvents were removed under reduced pressure and the residue was purified over silica gel using hexane/EtOAc (1 : 1) to give 8 (66 mg, 46%) as a white powder. $^1$H NMR (400 MHz, $CDCl_3$): δ 9.88 (s, 1H), 8.64 (s, 1H), 8.16 (dd, $J$ = 8.1 Hz, 1.4 Hz, 1H), 7.39 (t, $J$ = 8.1 Hz, 1H), 7.19 (dd, $J$ = 8.1 Hz, 1.4 Hz, 1H), 4.76 (t, $J$ = 5.3 Hz, 2H), 3.97 (s, 3H), 3.85 (t, $J$ = 5.3 Hz, 2H), 3.68 (t, $J$ = 6.2 Hz, 2H), 3.35 (t, $J$ = 6.2 Hz, 2H), 2.18–2.08 (m, 9H), 1.78–1.67 (m, 6H). $^{13}$C NMR (100 MHz, $CDCl_3$): δ 176.2, 150.9, 149.9, 125.2, 119.5, 114.3, 71.2, 70.4, 58.7, 56.4, 51.6, 41.8, 36.6, 29.9, 29.6. HRMS calcd for $C_{25}H_{32}BrN_2O_4$ (M+H) 503.1540, found 503.1539.

Synthesis of *N*-(1-adamantyl)-1-(2-(2-fluoroethoxy)ethyl)-8-methoxy-4-oxo-1,4-dihydroquinoline-3-carboxamide (RS-126). To a stirred solution of acetonitrile (1 mL), potassium fluoride (9.23 mg, 0.159 mmol) and Kryptofix (59.8 mg, 0.159 mmol) were added. The reaction mixture was heated to 90 °C, then compound 8 (20 mg, 0.040 mmol) was added and the mixture was stirred for 3 h. After cooling to ambient temperature, water (25 mL) was added and the mixture was extracted with EtOAc (3 × 5 mL). The combined organic layers were dried over $MgSO_4$ and solvents were removed under reduced pressure. The residue was purified over silica gel using hexane/EtOAc (3 : 2 to 1 : 2) to give RS-126 (4 mg, 23%) as a yellowish powder. $^1$H NMR (400 MHz, $CDCl_3$): δ 9.90 (s, 1H), 8.66 (s, 1H), 8.17 (dd, $J$ = 8.1 Hz, 1.4 Hz, 1H), 7.39 (t, $J$ = 8.1 Hz, 1H), 7.19 (d, $J$ = 7.7 Hz, 1H), 4.77 (t, $J$ = 4.9 Hz, 2H), 4.54–4.40 (m, 2H), 3.97 (s, 3H), 3.88 (t, $J$ = 4.9 Hz, 2H), 3.68–3.59 (m, 2H), 2.22–2.08 (m, 9H), 1.78–1.67 (m, 6H). $^{13}$C NMR (100 MHz, $CDCl_3$): δ 178.7, 150.9, 84.1, 82.5, 70.3, 65.5, 56.8, 56.4, 52.4, 41.7, 36.5, 29.5, 25.0, 17.0. HRMS calcd for $C_{25}H_{32}FN_2O_4$ (M+H) 443.2341, found 443.2340.

## Radiochemistry

[$^{18}$F]-fluoride was produced *via* the $^{18}$O(p,n)$^{18}$F nuclear reaction by bombardment of 98% enriched $^{18}$O-water using a Cyclone 18/9 cyclotron (18-MeV; IBA, Belgium). Aqueous $^{18}F^-$ was trapped on a hydrophilic anion exchange cartridge (Waters SepPak Accell QMA cartridge carbonate) and eluted with a tetrabutylammoniumhydroxide solution (TBAOH, 0.2 M in MeOH, 1 mL) into a reaction vessel. The solvents were evaporated at 90 °C under reduced pressure with a gentle inflow of nitrogen gas. After addition of acetonitrile (1 mL), azeotropic drying was carried out. This procedure was repeated twice to afford dry [$^{18}$F]TBAF complex. A solution of precursor compound 8 (1 mg, 2 μmol) in DMF (0.3 mL) was added and the reaction mixture was stirred at 110 °C for 10 min. After dilution with water (2.7 mL), the crude product was purified by semi-preparative HPLC system. The collected product fraction was diluted with water (10 mL), trapped on a C18 cartridge (Waters, preconditioned with 5 mL EtOH and 10 mL water), washed with water (5 mL), and eluted with EtOH (0.5 mL) through a sterile filter (0.2 μm). The volume of EtOH was decreased under reduced pressure until ca. 0.1 mL and water (2 mL) was added to give a final EtOH concentration of 5%. The total synthesis time from end of bombardment was 90 min. For quality control, an aliquot of the formulated solution was analyzed using the analytical HPLC system. The identity of the $^{18}$F-labeled product was confirmed by comparison with the HPLC retention time of the non-radioactive reference compound RS-126 and by co-injection. Specific radioactivity of the product was calculated by comparison of UV peak intensity with a calibration curve of the non-radioactive reference compound.

## *In vitro* binding assay

Membrane preparations obtained from CHO-K1 cells stably transfected with human CB1 or CB2 (PerkinElmer, 0.5 μg/tube for hCB1 and hCB2) were incubated at 30 °C for 90 min with increasing concentrations of test compounds (1 pM to 10 μM). [$^3$H]CP-55,940 (1.4 nM; PerkinElmer) was used as radioligand, an agonist with $K_i$ values of 0.58 nM and 0.69 nM toward hCB1 and hCB2, respectively. Non-specific binding was defined by the presence of 5 μM WIN-55212-2 (Biotrend AG; $K_i$ hCB1 = 1.89, $K_i$ hCB2 = 0.28 nM). Inhibition constants $K_i$ values were calculated using the Cheng–Prusoff equation. $K_D$ values of 0.14 and 0.11 nM from PerkinElmer were used for calculations for [$^3$H]CP-55,940 binding to hCB1 and hCB2 receptors, respectively.

For the murine CB2 binding affinity, an adapted protocol using membrane preparations from CHO cells expressing murine CB2 receptors in conjunction with [$^3$H]CP-55,940 was used. Binding was performed in 0.2 mL buffer pH 7.4 containing 50 mM tris(hydroxymethyl)aminomethane (Tris), 5 mM $MgCl_2$, 2.5 mM ethylene glycol tetraacetic acid (EGTA) and 0.1% fatty acid free bovine serum albumin (BSA) for 1 h at 30 °C under light shaking. The reaction was terminated by rapid filtration through microfiltration plates coated with 0.5% polyethylenimine (UniFilter GF/B filter plate; Packard, Perkin Elmer, Wokingham, UK). Bound radioactivity was analyzed for $K_i$ using nonlinear regression analysis (Activity Base; ID Business Solution, Limited, Guilford, UK).

## Animals

Animal care and experiments were conducted in accordance with Swiss Animal Welfare legislation and were approved by the Veterinary Office of Canton Zurich, Switzerland. Five-weeks old male Wistar (Crl:WI) rats and 5-weeks old male CD1 (Crl:CD1) mice were supplied by Charles River (Sulzfeld, Germany).

## *In vitro* stability studies

The stability of [$^{18}$F]RS-126 was investigated in rat and human plasma and in rat and mouse brain homogenates at 37 °C at various incubation times (0–120 min). Phosphate-buffered saline (PBS, 0.15 M, pH 7.4) was used as a control.

For plasma, [$^{18}$F]RS-126 formulated solution (10 μL, 3 MBq) was added to PBS (300 μL), rat (300 μL), and human plasma (300 μL), respectively. The mixtures were vortexed and incubated at 37 °C under shaking. An aliquot of 100 μL from each sample was taken at different time points (30, 60 and 120 min) and mixed with 100 μL ice-cooled acetonitrile and centrifuged (3 min, 4500 *g*). The supernatants were analyzed by radio-TLC Instant Imager (Packard, Canberra Company, Meriden, Connecticut, USA) using hexane/EtOAc (1 : 4) as the eluent.

For the *in vitro* stability studies of [$^{18}$F]RS-126 in the brain of a rat and mouse, whole brains were removed after decapitation and stored at −80 °C until use. For the actual experiment, the brains were thawed

and homogenized in PBS (3 mL; GIBCO Lucerne, Switzerland) with a polytron on ice. The homogenates (400 μL) were incubated with [$^{18}$F]RS-126 (15 μL, 7 MBq) at 37 °C under light shaking. An aliquot (100 μL) was taken at 15, 30, 60 and 120 min and mixed with ice-cooled acetonitrile (100 μL). The samples were vortexed, centrifuged (5 min, 4500 *g*) and the supernatants analyzed by radio-HPLC and radio-TLC using hexane/EtOAc (1 : 4) as the eluent.

### *In vitro* autoradiography

Rat spleen tissue embedded in TissueTek was cut into 20 μm thick sections on a cryostat (Cryo-Star HM 560 MV; Microm, Thermo Scientific, Wilmington, DE, USA). The slices were absorbed on SuperFrost Plus slides (Menzel, Braunschweig, Germany) and stored at −80 °C until use. For the experiment, the slices were thawed on ice and preconditioned at 0 °C in buffer (pH 7.4) containing 50 mM TRIS/HCl and 5% BSA (incubation buffer). The tissue slices were dried and then incubated with 600 μL incubation buffer containing [$^{18}$F]RS-126 (0.6 nM) for 15 min at 21°C in a humid chamber. Under blockade conditions, AM251 (5 μM, CB1 inverse agonist, low CB2 binding affinity, $K_i$ = 2.3 μM) or GW405833 (5 μM, CB2 inverse agonist, high CB2 binding affinity, $K_i$ = 3.9 nM) was added to the incubation buffer containing the radioligand. The slices were washed with washing buffer (50 mM TRIS/HCl, 1% BSA, 5% EtOH, pH 7.4) for 2 min (2×) and with distilled water for 5 s (2×) on ice. After drying, the slices were exposed (30 min) to appropriate phosphor imager plates (Fuji, Dielsdorf, Switzerland) and the films were scanned in a BAS5000 reader (Fuji).

### Determination of LogD7.4

The shake-flask method was used to determine the partition coefficient D. In brief, *n*-octanol saturated with phosphate buffer pH 7.4 (0.5 mL) and phosphate buffer saturated with *n*-octanol (0.5 mL) were mixed with [$^{18}$F]RS-126 (20 μL). The samples were shaken for 15 min and centrifuged at 5000 *g* for 5 min at 21°C. Layers were separated and radioactivity in each layer was measured in a gamma counter (Wizard; PerkinElmer). LogD is expressed as the logarithm of the ratio between the radioactivity concentrations (Bq/mL) of the octanol and the buffer phase.

### *Ex vivo* metabolic stability

The radiotracer was administered intravenously to Wistar rats ($n$ = 2, 251 g and 330 g, 100 and 124 MBq, respectively, 1–4 nmol) by tail vein injection. From the first rat (251 g), blood samples were withdrawn from the tail artery at 15, 30 and 45 min p.i.. The rat was killed by decapitation at 60 min p.i. to collect blood, spleen, and brain. Blood from the second rat (330 g) was collected from the tail artery at 5 min p.i.. The rat was killed 15 min p.i. to collect blood, spleen, and brain. All the blood samples were collected in heparin-coated tubes (BD Vacutainers, Allschwil, Switzterland) and centrifuged at 5000 *g* for 5 min at 4 °C. The proteins of the plasma were precipitated by addition of an equal volume of ice-cooled acetonitrile and centrifuged at 5000 *g* for 5 min. The spleen and brain tissues were homogenized in PBS (2 mL) for 2 min with a polytron. Ice-cooled acetonitrile (2 mL) was added to precipitate proteins followed by centrifugation at 5000 *g* for 5 min. Supernatants were analyzed by radio-TLC using hexane/EtOAc (1 : 4). Results are expressed as percentage of the radioactivity of intact parent compound from total radioactivity.

### *Ex vivo* biodistribution studies

For biodistribution studies, a formulated solution of [$^{18}$F]RS-126 (6–15 MBq, 0.06–0.16 nmol) was administered *via* tail vein injection into Wistar rats ($n$ = 3, 316–355 g). For blocking conditions, GW405833 (1.5 mg/kg) was injected intravenous shortly before radiotracer injection ($n$ = 3, 330–356 g). For *in vivo* applications, 1.5 mg GW405833 was dissolved in 1 mL solution containing 10% ethanol, 2% cremophor, and 88% water for injection. Animals were euthanzised under anesthesia with isoflurane by decapitation at 10 min p.i. Blood and tissues were collected, weighed, and radioactivity measured in a gamma-counter (Wizard; PerkinElmer). The accumulated radioactivity in the tissues was expressed as percentage of injected dose per gram wet tissue normalized to 1 kg body weight of the animals (norm. %ID/g tissue).

### *In vivo* rat spleen-PET imaging

For rat spleen-PET scans, animals ($n$ = 9, 260–400 g) were anesthetized with isoflurane and 10–17 MBq (0.3–0.5 nmol) [$^{18}$F]RS-126 was injected *via* the tail vein. Depth of anesthesia was monitored by measuring respiratory frequency (SA Instruments, Inc., Stony Brook, NY, USA). Body temperature was controlled by a rectal probe and kept at 37 °C by a thermocoupler and a heated air stream. Rats under baseline ($n$ = 5) and displacement ($n$ = 4) conditions were scanned for 90 min in dynamic PET acquisition mode. Rats in the displacement experiment additionally received 1.5 mg/kg GW405833 intravenously 10 min after radiotracer injection respectively to the start of PET acquisition. PET data were reconstructed in user-defined time frames with a voxel size of 0.3875 × 0.3875 × 0.775 mm$^3$ by two-dimensional-ordered subsets expectation maximization. Random and single but no attenuation correction was applied. PET acquisitions were followed by a CT for anatomical orientation. Image files were analyzed with PMOD 3.6 software (PMOD Technologies Ltd., Zurich, Switzerland). Spleen and muscle regions were defined manually and tissue radioactivity was expressed as standardized uptake values (SUVs), that is, the decay-corrected radioactivity per cm$^3$ divided by the injected radioactivity dose per gram of body weight.

### *In vivo* mouse brain-PET imaging after lipopolysaccharide-induced neuroinflammation

Male CD1 mice (28–36 g) were intraperitoneally injected with 10 mg/kg lipopolysaccharide (LPS; *E. coli* strain O111:B4, Sigma L4130; Sigma, St Louis, MO, USA, dissolved in 0.9% NaCl, $n$ = 11) or vehicle (0.9% NaCl, $n$ = 6) 5 or 7 days prior brain-PET imaging. For blocking experiments, LPS-treated mice received 2 mg/kg GW405833 subcutaneously 30 min before radiotracer administration ($n$ = 5). All other mice ($n$ = 12) received an injection of the vehicle solution (10% ethanol, 2% Cremophor, 88% water for injection). Mice were intravenously administered with 3–11 MBq (0.1–0.3 nmol) [$^{18}$F]RS-126 and PET acquisition was started simultaneous with injection. Dynamic PET scans lasted for 60 min and were followed by CT acquisition. Mouse monitoring and PET data reconstruction was performed as described above. Time activity curves (TACs) of the brain regions, defined on the mouse MRI T2 template (PMOD Technologies Ltd.), were calculated and expressed as SUVs.

### Statistics

For each group, the mean value was calculated and expressed with standard deviation or standard error. Differences in mean values were evaluated by an unpaired two-tailed student's *t*-test (GraphPad Prism 6.0 software; GraphPad Software Inc., San Diego, CA, USA). A $p$-value $< 0.05$ was considered significant.

## Results

### Chemistry

Based on the core structure of RS-016, which was previously labeled in our group with carbon-11 (Slavik *et al.* 2015b), three novel fluorinated analogs of RS-016 were designed (Fig. 1) and synthesized.

Compound RS-030 was synthesized following a similar synthetic procedure described for RS-016 (Slavik *et al.* 2015b) starting from commercially available anisidine and diethyl 2-(ethoxymethylene)malonate as shown in Scheme 1. Compound 2 was prepared via the Gould–Jacobs reaction at high temperatures. *N*-alkylation under basic conditions afforded compound 3 in 75% yields. Quinoline acid 4 was obtained by saponification of the ethyl ester 3 with 10% sodium hydroxide. Amide bond formation using HBTU as the coupling reagent provided compound RS-028 in a good yield (84%). The alcohol was subsequently reacted with DAST according to a previously reported patent (Jasys and Volkmann 2000) to afford the desired fluorinated analog RS-030 in an overall yield of 30%.

Compound 5 in Scheme 2 was obtained after demethylation of RS-016 using lithium chloride. The introduction of the fluoroethyl side chain was achieved by *O*-alkylation of compound 5 with fluoroethyl tosylate to yield the desired fluoroethoxy derivative RS-122 in 79% yield.

Saponification of compound 2 with 10% NaOH (Scheme 3) yielded carboxylic acid 6, which was subsequently coupled with 1-aminoadamantane to afford compound 7. *N*-alkylation of compound 7 using bis(2-bromoethyl)ether gave compound 8 in 46% yield, which was then fluorinated with KF-Kryptofix to yield the fluoroethyl ether derivative RS-126 in 23% yield.

### *In vitro* binding affinity studies

The three novel fluorinated analogs of RS-016 were investigated for their binding affinities toward CB2 and selectivity over CB1. Competitive binding experiments were carried out with each candidate compound using [$^3$H]CP55940, a well-characterized CB1/CB2 agonist, and employing membranes prepared from cells expressing human CB1 or CB2 receptors. Non-radioactive WIN-55212-2 was used for the determination of non-specific binding. The displacement curves showing the averaged values of three $IC_{50}$ measurements are depicted in Figure S1. The inhibition constants ($K_i$) of all the

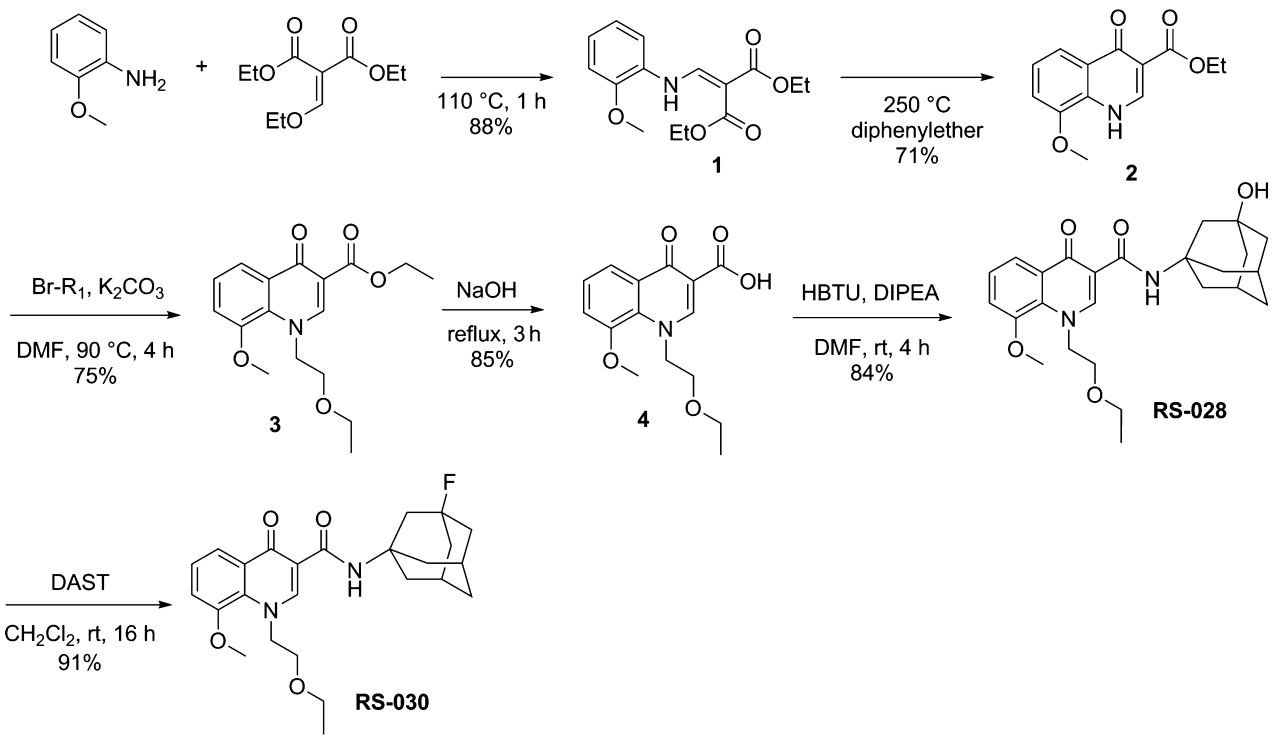


**Scheme 1** Synthesis of 3-fluoroadamantyl derivative RS-030. DAST, *N,N*-diethylaminosulfur trifluoride; HBTU, *O*-(benzotriazol-1-yl)-*N,N,N′,N′*-tetramethyluronium hexafluorophosphate.

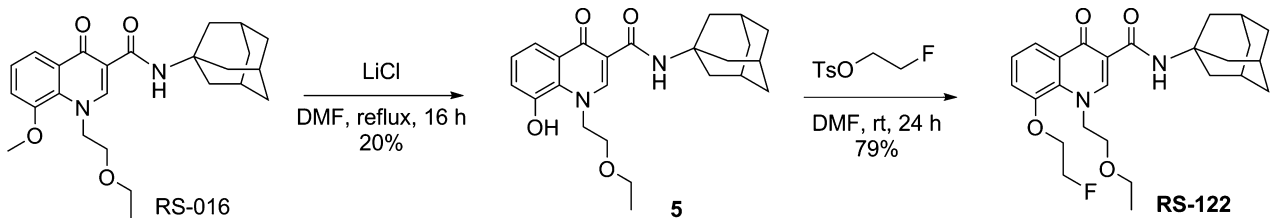


**Scheme 2** Synthesis of fluoroethoxy derivative RS-122.

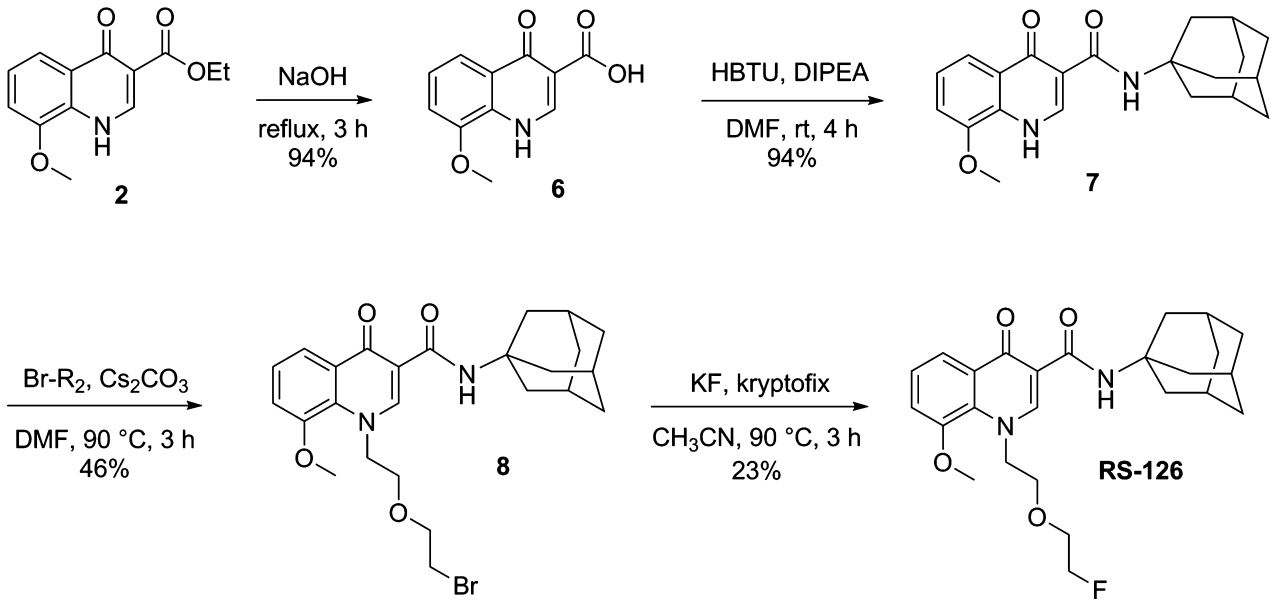


**Scheme 3** Synthesis of fluoroethyl ether derivative RS-126.

tested compounds RS-030, RS-122, and RS-126 (Table 1) were estimated using the Cheng–Prusoff equation.

The replacement of the adamantyl group with the fluorinated adamantyl moiety yielded RS-030 with a favorable $K_i$ value of 2.1 nM toward CB2. Substitution of the methoxy group in RS-016 with fluoroethyl resulted in RS-122, which showed a 100-fold loss in affinity toward CB2 ($K_i$ 72 nM). The 2-fluoroethyl derivative RS-126 ($K_i$ 1.2 nM) represents the most potent CB2 ligand of all the three ligands investigated, indicating that bioisosteric replacement of a proton with a fluorine atom in the ethyl side chain does not affect CB2 affinity. This potent CB2 ligand exhibited > 8000-fold ($K_i$ CB1 > 10 μM) selectivity over CB1. In a further experiment using membranes expressing mouse CB2, a $K_i$ value of 4.5 nM was obtained for RS-126. This result is comparable to the human CB2 $K_i$ value of 1.2 nM, indicating no significant species differences.

## Radiosynthesis

[$^{18}$F]RS-126 was prepared *via* nucleophilic substitution of the bromo precursor 8 with [$^{18}$F]TBAF (Scheme 4) and the fluorinated crude product was purified by semi-HPLC. In a typical experiment, a moderate radiochemical yield of ~ 6% (decay corrected) was achieved with a radiochemical purity > 99%. The average specific activity for [$^{18}$F]RS-126 was 98 GBq/μmol at the end of the radiosynthesis. The identity of the radiolabeled compound was confirmed by co-injection with the non-radioactive reference compound RS-126.

## *In vitro* characterization of [$^{18}$F]RS-126

The shake-flask method was applied to measure the distribution of [$^{18}$F]RS-126 in *n*-octanol/phosphate buffer (pH 7.4). The obtained $\log D_{7.4}$ value of 1.99 ± 0.02 ($n$ = 5) suggests that [$^{18}$F]RS-126 is sufficiently lipophilic for free diffusion across the blood–brain barrier (Dishino *et al.* 1983).

The radiotracer was chemically stable for up to 2 h (data not shown). Plasma stability tests were carried out in rat and human plasma over a period of 120 min at 37 °C. No radioactive degradation or biotransformation products of [$^{18}$F]RS-126 were detected in human or rat plasma after 120 min incubation time.

**Table 1** Binding affinity ($K_i$) values of known cannabinoid ligands and novel fluorinated derivatives with RS-016 as lead structure.

| Compound | $K_i$ CB1 [nM] | $K_i$ CB2 [nM] | References |
|---|---|---|---|
| *AM251* | 7.49 | 2290 | Lan *et al.* 1999 |
| *WIN-55212-2* | 1.89 | 0.28 | Showalter *et al.* 1996 |
| *CP-55,940* | 0.58 | 0.69 | Showalter *et al.* 1996 |
| *GW405833* | 4772 | 3.90 | Valenzano *et al.* 2005 |
| *RS-016* | > 10 000 | 0.7 ± 0.6 | Slavik *et al.* 2015b |
| *RS-030* | > 10 000 | 2.1 ± 1.5 | This work ($n$ = 3) |
| *RS-122* | > 10 000 | 72 ± 102 | This work ($n$ = 3) |
| *RS-126* | > 10 000 | 1.2 ± 0.8 | This work ($n$ = 3) |

Brain homogenates from rat and mouse were incubated with [$^{18}$F]RS-126 at 37 °C under light shaking. After 120 min of incubation time, 97% and 98% of the total radioactivity was assigned to the intact parent compound in the rat and mouse brain samples, respectively.

Autoradiography images showed high radioactivity accumulation of [$^{18}$F]RS-126 to rat spleen tissue, an organ with high basal levels of CB2 receptors, under baseline conditions (Fig. 2). Blocking experiments using rat spleen slices that were co-incubated with [$^{18}$F]RS-126 and the CB2 inverse agonist GW405833 (5 μM, $K_i$ toward CB2 = 3.9 nM, $K_i$ toward CB1 = 4772 nM (Valenzano *et al.* 2005)) displayed a substantially reduced radioactive signal. Co-incubation of [$^{18}$F]RS-126 with an excess amount of the CB1 inverse agonist AM251 (5 μM, $K_i$ toward CB2 = 2.3 μM (Lan *et al.* 1999)) using rat spleen slices showed similar intensity of radioactive signal as under baseline conditions, indicating selectivity of [$^{18}$F]RS-126 for CB2 over CB1.

### *Ex vivo* metabolic stability of [$^{18}$F]RS-126 in rats

The *ex vivo* metabolic fate of [$^{18}$F]RS-126 was studied using healthy rat blood plasma, spleen, and brain. In spleen samples, 81% and 75% of the total radioactivity were assigned to the intact parent compound at 15 and 60 min p.i., respectively. In blood plasma samples, only one radiometabolite, which was more hydrophilic than [$^{18}$F]RS-126, was detected. The percentage of intact compound in blood plasma decreased to 82% at 5 min p.i., 55% at 10 min p.i., 33% at 30 min p.i., 31% at 45 min p.i. and 23% at 60 min p.i.. In brain samples, negligible radioactivity was detected, which did not permit data evaluation. In the above section, we already proved that *in vitro* incubation of [$^{18}$F]RS-126 with rat and mouse brain homogenates emerged no biotransformation of the parent radioligand.

### *In vivo* PET imaging of peripheral CB2 in rat spleen with [$^{18}$F]RS-126

*In vivo* accumulation of [$^{18}$F]RS-126 in the CB2-positive rat spleen was investigated by PET imaging (Fig. 3). The spleen was clearly visible during the first 19 min after [$^{18}$F]RS-126 injection (baseline). For displacement studies, the time point for injection of the CB2-selective agonist GW405833 was chosen at 10 min post radiotracer injection because at that point, spleen-radioactivity was still high enough to be displaced and was markedly discriminated from the background. The radioactivity in the spleen decreased more rapidly after [$^{18}$F]RS-126 displacement and visible in the second time frame (10–19 min). The specific spleen-binding of [$^{18}$F]RS-126 which was measured within the first 9 min was successfully displaced after administration of GW405833. The corresponding TACs from spleen and muscle of baseline and displacement experiments are shown in Figure S2. Clearance of [$^{18}$F]RS-126 from spleen tissue was considerably enhanced after administration of the displacer. The spleen-TAC reached background levels approx. 5 min after displacer injection.

### *Ex vivo* biodistribution of [$^{18}$F]RS-126 in rats

Figure 4 shows the biodistribution data of [$^{18}$F]RS-126 in rats at 10 min post injection. The highest accumulation of radioactivity was found in the liver, spleen, and small intestine followed by adrenal glands and kidneys. The low uptake of radioactivity in the bone suggests that no significant defluorination has occurred during the experiment. To assess the specificity of [$^{18}$F]RS-126 uptake in CB2-positive organs such as the spleen, the CB2 receptor specific ligand GW405833 was utilized as a blocking agent. As shown in Fig. 4, a significant reduction of radioactivity uptake by 79% ($p$ = 0.008) was observed for [$^{18}$F]RS-126 in the spleen tissue, indicating high specific binding of [$^{18}$F]RS-126 to peripheral CB2. Besides the spleen, a significant reduction of radioactivity was found in the blood and lung after GW405833 administration. It has been reported that lung (Brown *et al.* 2002) and blood cells (Galiegue *et al.*

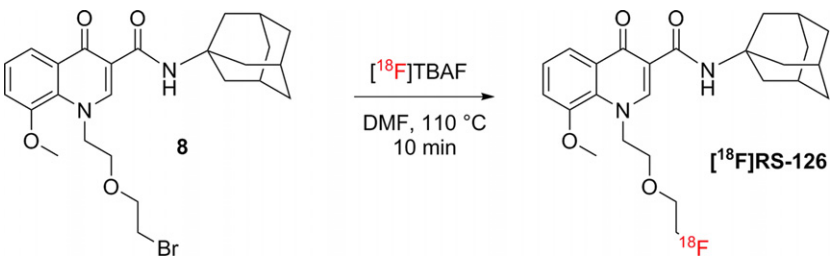


**Scheme 4** Radiosynthetic scheme for the preparation of [$^{18}$F]RS-126. TBAF, tetra-*n*-butylammonium fluoride.

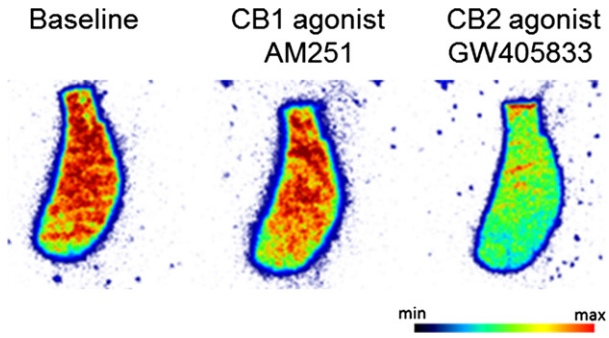


**Fig. 2** Representative *in vitro* autoradiograms of rat spleen tissues after incubation with [$^{18}$F]RS-126 under baseline and blocking conditions (5 μM cannabinoid receptor type 1 (CB1) agonist AM251 or 5 μM CB2 agonist GW405833).

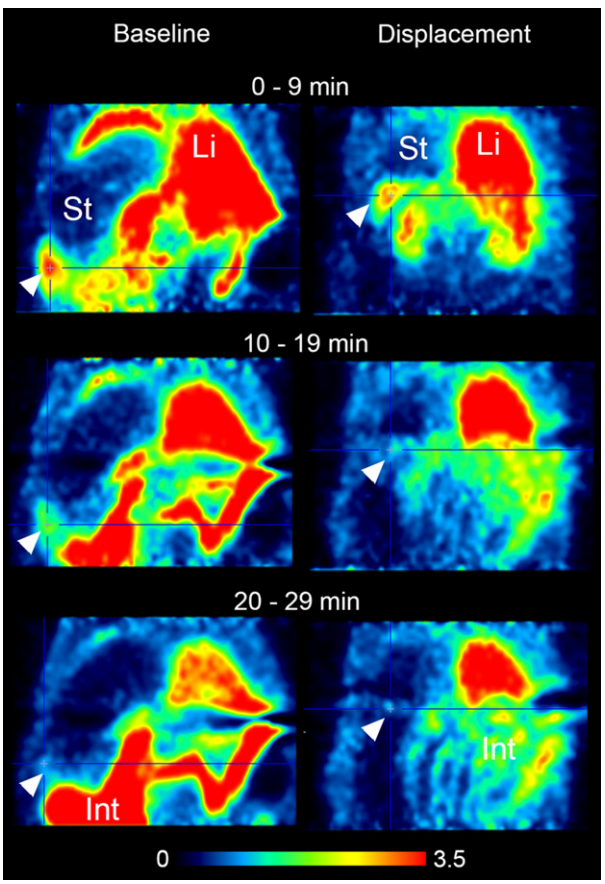


**Fig. 3** Representative coronal positron emission tomography (PET) images showing the abdominal region of two rats after [$^{18}$F]RS-126 injection under baseline and displacement (1.5 mg/kg cannabinoid receptor type 2 (CB2)-selective agonist GW405833 injected 10 min after radiotracer) conditions. PET images were averaged to three time frames as indicated. White arrowhead indicates the spleen. Injection of GW405833 at 10 min displaced [$^{18}$F]RS-126 from spleen tissue, which is no more visible in the last two time frames (right column). St, stomach; Li, liver; Int, intestine. Color bar indicates standardized uptake values (SUV).

1995) do express CB2, however, at much lower levels than spleen. The high standard deviation of the small intestine in blockade group is addressed to one animal (animal no. 1 in Table S1) with very high radiotracer uptake for which we have no explanation so far. Absolute values for each animal are listed in Table S1.

### *In vivo* brain-PET of CB2 in a mouse model of neuroinflammation using [$^{18}$F]RS-126

In our previous studies, a LPS-induced neuroinflammation mouse model was used to study radiotracer uptake and binding to the brain (Slavik *et al.* 2015a,b). CB2-mRNA levels increased in the mouse brain 5 days after LPS treatment (Slavik *et al.* 2015b). In this work, mice were injected with 10 mg/kg LPS 5 or 7 days prior [$^{18}$F]RS-126 PET imaging (Fig. 5). Control animals were administered with 0.9% NaCl (vehicle). However, compared to control animals, we did not find an increased accumulation of [$^{18}$F]RS-126 in the brains of LPS-treated mice neither at 5 nor 7 days post treatment. Additionally, 2 mg/kg GW405833 was subcutaneously injected 30 min prior [$^{18}$F]RS-126 administration. Brain-TACs of this group showed the same course as the other two groups. TACs of individual brain regions (e.g. cortex, striatum, hippocampus cerebellum etc.) were analyzed, however, with a similar result as shown for the whole brain (data not shown). Defluorination was observed 30 min after radiotracer injection, which led to incorporation of radioactivity in the cranial bone and increased SUV in whole brain-TACs (Fig. 5) because of spillover of radioactivity.

## Discussion

RS-016, which was previously prepared in our laboratory, exhibits high binding affinity toward CB2 ($K_i$ = 0.7 nM), good selectivity over CB1 ($K_i$ > 10 μM), and an appropriate lipophilicity ($\log D_{7.4}$ = 2.78) for brain penetration (Slavik *et al.* 2015b). Unfortunately, its structure only allows for radiolabeling with carbon-11, an isotope with a relatively short physical half-life of 20.3 min. In this study, three novel fluorinated analogs of RS-016 were designed and synthesized. The 3-fluoroadamantyl derivative RS-030 was prepared from the 3-hydroxyadamantyl intermediate RS-028 using DAST as the fluorinating agent. RS-122 was obtained in 79% yield by treatment of the cesium salt of the phenolic precursor 5 with fluoroethyl tosylate. The fluoroethyl ether derivative RS-126 was obtained by reacting the bromo precursor 8 with potassium fluoride and kryptofix. The yield of this reaction was relatively low (23%) probably because of a competing elimination reaction. Since sufficient amount of RS-126 was obtained for *in vitro* evaluation, no efforts were undertaken to optimize the chemical yield. From all the fluorinated analogs of RS-016 synthesized, compound RS-126 exhibited the highest binding affinity ($K_i$ = 1.2 nM) to CB2 and was therefore selected for further evaluation.

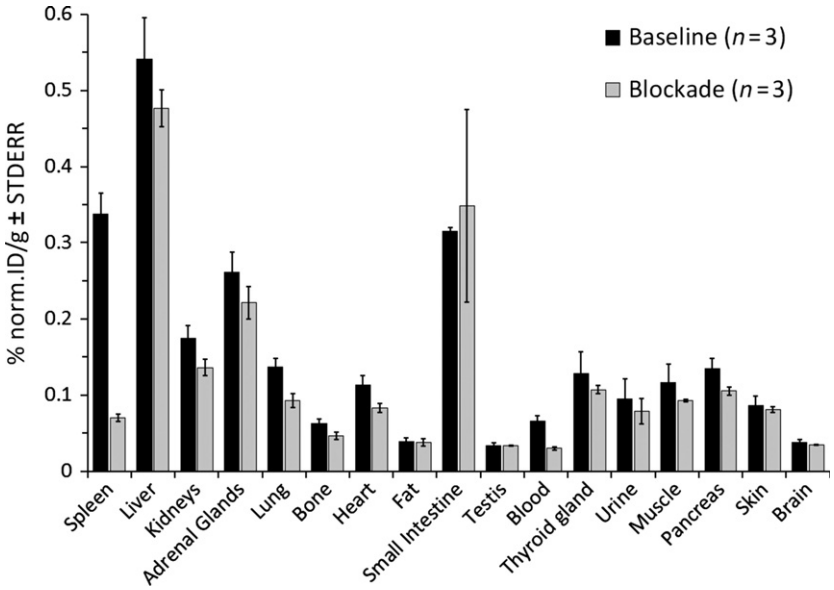


**Fig. 4** Radioactivity accumulation of [$^{18}$F]RS-126 in selected rat tissue 10 min post injection under baseline (black bars) and blocking (gray bars; pre-administration of 1.5 mg/kg GW405833) conditions. Data are presented as the mean of the percentage of injected dose per gram tissue normalized to the body weight (kg) of the animals ± standard error [% norm. ID/g tissue, means ± standard error ($n$ = 3)]. Absolute values are listed in Table S1.

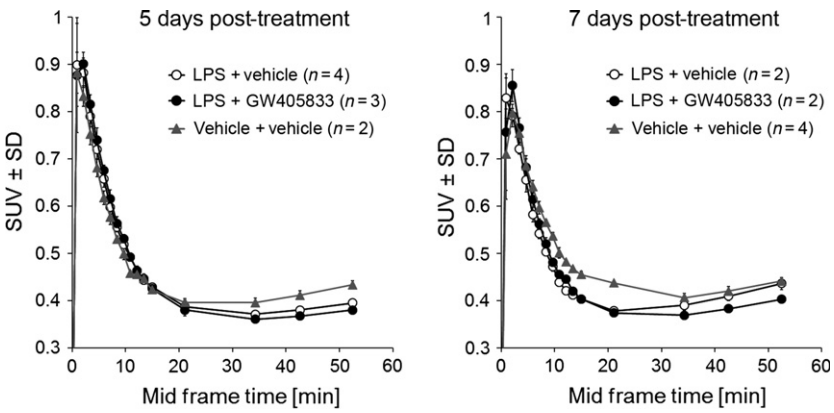


**Fig. 5** Whole brain [$^{18}$F]RS-126 time activity curves in a LPS-induce neuroinflammatory mouse model. Mice were intraperitoneal administered with 10 mg/kg LPS or vehicle (0.9% NaCl). [$^{18}$F]RS-126 PET imaging was performed at 5 or 7 days post treatment. Mice were further injected with 2 mg/kg GW405833 or the corresponding vehicle subcutaneous 30 min prior PET acquisition. Note: Increasing SUV values from 30 min onwards are attributed to defluorination of [$^{18}$F]RS-126 followed by accumulation in the cranial bone and spill over to the brain.

For the radiolabeling of RS-126 with fluorine-18, we initially used $K_{2.2.2}$/K[$^{18}$F]F complex as the fluorinating reagent, but very low radiochemical yields (< 1%) were obtained under various radiolabeling conditions. Increasing the reaction temperature as well as varying the reaction solvent and reaction time using $K_{2.2.2}$/K[$^{18}$F]F complex as the fluorinating reagent did not significantly improve the radiochemical yield. Treatment of the bromide precursor 8 with [$^{18}$F]TBAF as the radiofluorination reagent in the presence of TBAOH as the base afforded target compound [$^{18}$F]RS-126 in 6% radiochemical yield. Replacing the more basic TBAOH by $TBAHCO_3$ with the aim to reduce potential elimination products also did not lead to any improvement in the radiochemical yield of [$^{18}$F]RS-126. In order to improve the radiochemical yield of [$^{18}$F]RS-126, we suggest to use a tosylate or mesylate precursor in future studies. A higher $^{18}$F-incorporation is expected because of the fact that tosyl or mesyl is a better leaving group compared to bromide.

The lipophilicity of [$^{18}$F]RS-126 was determined using the shake-flask method and gave a $logD_{7.4}$ value of 1.99, which is lower than the $logD_{7.4}$ value of [$^{11}$C]RS-016 (2.78). This value is still within the optimal lipophilicity range of 1–3 for brain-penetrating compounds. Autoradiographic studies with [$^{18}$F]RS-126 showed high specific binding to CB2-positive rat spleen tissue sections. Compared to [$^{11}$C]RS-016, similar *in vitro*/*ex vivo* metabolite stabilities were observed for [$^{18}$F]RS-126. No degradation product was detected in *in vitro* assays with rat or human plasma. *In vivo*, rat spleen samples revealed 81% of the intact parent compound at 15 min post injection, which is similar to the value obtained for [$^{11}$C]RS-016 at 20 min p.i.. *In vivo* displacement studies confirmed selective binding of [$^{18}$F]RS-126 to CB2 in the rat spleen. Biodistribution studies with rats revealed 79% specific binding of [$^{18}$F]RS-126 to spleen tissue. Based on the results we previously obtained with [$^{11}$C]RS-016 in LPS-treated mice, we anticipated similar results with [$^{18}$F]RS-126. However, contrary to our expectations, we could not detect CB2 expression

in the brains of LPS-treated mice. Considering the cold mass injected to LPS-treated mice which was based on specific radioactivity calculations, a 5–7.5-fold higher RS-126 (0.1–0.3 nmol) was injected to LPS-treated mice compared to RS-016 (0.02–0.04 nmol). In addition, we found a lower gene expression level of CB2 in LPS-treated mice of 6.5-fold compared to 9.5-fold from our previous study with [$^{11}$C]RS-016. We thus speculate that the lower specific activity of [$^{18}$F]RS-126 (98 GBq/μmol compared to [$^{11}$C]RS-016 with 545 GBq/μmol) hampers the detection by PET of the per se moderate CB2 levels in the brains of LPS-treated mice. Another drawback is the rapid *in vivo* metabolism of [$^{18}$F]RS-126 in mice which resulted in the formation of [$^{18}$F]fluoride. Based on these results, we cannot definitely conclude that [$^{18}$F]RS-126 crosses the blood–brain barrier. However, we assume some permeation of [$^{18}$F]RS-126 into the brain since the structurally related [$^{11}$C]KD2 (Mu *et al.* 2013) showed moderate brain uptake in *in vitro* transport experiments.

## Conclusion

[$^{18}$F]RS-126 was successfully produced in a one-step nucleophilic substitution reaction using [$^{18}$F]TBAF as the radiofluorination reagent. No degradation product was observed when [$^{18}$F]RS-126 was incubated in rat or human plasma for up to 2 h at 37 °C. High binding to CB2-positive tissue was demonstrated in autoradiographic studies *in vitro* using rat spleen sections. *In vivo* specificity toward spleen-CB2 was also demonstrated in displacement and biodistribution experiments. Using a mouse model of LPS-induced neuroinflammation, we were not able to detect elevated CB2 levels in the brain by [$^{18}$F]RS-126-PET imaging. This could be attributed to the specific activity of [$^{18}$F]RS-126 and the moderately enhanced CB2 expression in LPS-treated mice brain. Nonetheless, the preclinical data on [$^{18}$F]RS-126 indicate that this new radioligand is a promising radiotracer for imaging CB2 receptors.

## Acknowledgments and conflict of interest disclosure

We thank Ms. Claudia Keller for performing *in vivo* studies. We also thank the Swiss ALS Foundation and the Vontobel Foundation for partly financing this project. The authors have no conflict of interest to declare.

All experiments were conducted in compliance with the ARRIVE guidelines.

## Supporting information

Additional Supporting Information may be found online in the supporting information tab for this article:

**Figure S1.** Displacement curves for compounds RS-030, RS-122, and RS-126 and compared with RS-016 using membranes expressing human CB2 receptors.

**Figure S2.** [$^{18}$F]RS-126 time activity curves of rat spleen (circle) and muscle (triangle) under baseline (n = 5) and displacement (1.5 mg/kg CB2-selective agonist GW405833, n = 4) conditions.

**Table S1.** [$^{18}$F]RS-126 biodistribution values in rat tissue at 10 min p.i. under baseline (n = 3) and blocking (n = 3; pre-administration of 1.5 mg/kg GW405833).

## References

Ametamey S. M., Honer M. and Schubiger P. A. (2008) Molecular imaging with PET. *Chem. Rev.* **108**, 1501–1516.

Benito C., Nunez E., Pazos M. R., Tolon R. M. and Romero J. (2007) The endocannabinoid system and Alzheimer's disease. *Mol. Neurobiol.* **36**, 75–81.

Benito C., Tolon R. M., Pazos M. R., Nunez E., Castillo A. I. and Romero J. (2008) Cannabinoid CB2 receptors in human brain inflammation. *Br. J. Pharmacol.* **153**, 277–285.

Boutin H., Chauveau F., Thominiaux C. *et al.* (2007) 11C-DPA-713: a novel peripheral benzodiazepine receptor PET ligand for in vivo imaging of neuroinflammation. *J. Nucl. Med.* **48**, 573–581.

Brown S. M., Wager-Miller J. and Mackie K. (2002) Cloning and molecular characterization of the rat CB2 cannabinoid receptor. *Biochim. Biophys. Acta* **1576**, 255–264.

Chauveau F., Boutin H., Van Camp N., Dolle F. and Tavitian B. (2008) Nuclear imaging of neuroinflammation: a comprehensive review of [11C]PK11195 challengers. *Eur. J. Nucl. Med. Mol. Imaging* **35**, 2304–2319.

Damont A., Marguet F., Puech F. and Dolle F. (2015) Synthesis and in vitro characterization of novel fluorinated derivatives of the TSPO 18 kDa ligand SSR180575. *Eur. J. Med. Chem.* **101**, 736–745.

Di Marzo V. (2009) The endocannabinoid system: its general strategy of action, tools for its pharmacological manipulation and potential therapeutic exploitation. *Pharmacol. Res.* **60**, 77–84.

Dishino D. D., Welch M. J., Kilbourn M. R. and Raichle M. E. (1983) Relationship between lipophilicity and brain extraction of C-11-labeled radiopharmaceuticals. *J. Nucl. Med.* **24**, 1030–1038.

Eljaschewitsch E., Witting A., Mawrin C. *et al.* (2006) The endocannabinoid anandamide protects neurons during CNS inflammation by induction of MKP-1 in microglial cells. *Neuron* **49**, 67–79.

Endres C. J., Pomper M. G., James M. *et al.* (2009) Initial evaluation of 11C-DPA-713, a novel TSPO PET ligand, in humans. *J. Nucl. Med.* **50**, 1276–1282.

Evens N., Bosier B., Lavey B. J. *et al.* (2008) Labelling and biological evaluation of [(11)C]methoxy-Sch225336: a radioligand for the cannabinoid-type 2 receptor. *Nucl. Med. Biol.* **35**, 793–800.

Evens N., Muccioli G. G., Houbrechts N., Lambert D. M., Verbruggen A. M., Van Laere K. and Bormans G. M. (2009) Synthesis and biological evaluation of carbon-11- and fluorine-18-labeled 2-oxoquinoline derivatives for type 2 cannabinoid receptor positron emission tomography imaging. *Nucl. Med. Biol.* **36**, 455–465.

Evens N., Vandeputte C., Coolen C. *et al.* (2012) Preclinical evaluation of [(11)C]NE40, a type 2 cannabinoid receptor PET tracer. *Nucl. Med. Biol.* **39**, 389–399.

Galiegue S., Mary S., Marchand J. *et al.* (1995) Expression of central and peripheral cannabinoid receptors in human immune tissues and leukocyte subpopulations. *Eur. J. Biochem.* **232**, 54–61.

Gao M., Xu J., Wang M. and Zheng Q. H. (2014) Facile and high-yield synthesis of N-(4-diethylamino)benzyl-4-[(1)(1)C]methoxy-N-(p-tolyl)benzenesulfonamide as a new potential PET selective CB2 radioligand. *Appl. Radiat. Isot.* **90**, 181–186.

Halldin C., Gulyas B. and Farde L. (2001) PET studies with carbon-11 radioligands in neuropsychopharmacological drug development. *Curr. Pharm. Des.* **7**, 1907–1929.

Honer M., Gobbi L., Martarello L. and Comley R. A. (2014) Radioligand development for molecular imaging of the central nervous system with positron emission tomography. *Drug Discovery Today* **19**, 1936–1944.

Horti A. G., Gao Y., Ravert H. T., Finley P., Valentine H., Wong D. F., Endres C. J., Savonenko A. V. and Dannals R. F. (2010) Synthesis and biodistribution of [11C]A-836339, a new potential radioligand for PET imaging of cannabinoid type 2 receptors (CB2). *Bioorg. Med. Chem.* **18**, 5202–5207.

Jasys V. J. and Volkmann R. A. (2000) *Fluoro-substituted adamantane derivatives*. Pfizer Inc, patent No. CA2234319 C, 1998.

Lan R., Liu Q., Fan P., Lin S., Fernando S. R., McCallion D., Pertwee R. and Makriyannis A. (1999) Structure-activity relationships of pyrazole derivatives as cannabinoid receptor antagonists. *J. Med. Chem.* **42**, 769–776.

Matsuda L. A., Lolait S. J., Brownstein M. J., Young A. C. and Bonner T. I. (1990) Structure of a cannabinoid receptor and functional expression of the cloned cDNA. *Nature* **346**, 561–564.

Merighi S., Gessi S., Varani K., Fazzi D., Mirandola P. and Borea P. A. (2012) Cannabinoid CB(2) receptor attenuates morphine-induced inflammatory responses in activated microglial cells. *Br. J. Pharmacol.* **166**, 2371–2385.

Mu L. J., Bieri D., Slavik R. *et al.* (2013) Radiolabeling and in vitro/in vivo evaluation of N-(1-adamantyl)-8-methoxy-4-oxo-1-phenyl-1,4-dihydroquinoline-3-carboxamide as a PET probe for imaging cannabinoid type 2 receptor. *J. Neurochem.* **126**, 616–624.

Mukhopadhyay S., Das S., Williams E. A., Moore D., Jones J. D., Zahm D. S., Ndengele M. M., Lechner A. J. and Howlett A. C. (2006) Lipopolysaccharide and cyclic AMP regulation of CB(2) cannabinoid receptor levels in rat brain and mouse RAW 264.7 macrophages. *J. Neuroimmunol.* **181**, 82–92.

Munro S., Thomas K. L. and Abu-Shaar M. (1993) Molecular characterization of a peripheral receptor for cannabinoids. *Nature* **365**, 61–65.

Owen D. R. and Matthews P. M. (2011) Imaging brain microglial activation using positron emission tomography and translocator protein-specific radioligands. *Int. Rev. Neurobiol.* **101**, 19–39.

Pertwee R. G. (2009) Emerging strategies for exploiting cannabinoid receptor agonists as medicines. *Br. J. Pharmacol.* **156**, 397–411.

Piel M., Vernaleken I. and Rosch F. (2014) Positron emission tomography in CNS drug discovery and drug monitoring. *J. Med. Chem.* **57**, 9232–9258.

Ruhl T., Deuther-Conrad W., Fischer S., Gunther R., Hennig L., Krautscheid H. and Brust P. (2012) Cannabinoid receptor type 2 (CB2)-selective N-aryl-oxadiazolyl-propionamides: synthesis, radiolabelling, molecular modelling and biological evaluation. *Org. Med. Chem. Lett.* **2**, 32.

Savonenko A. V., Melnikova T., Wang Y. *et al.* (2015) Cannabinoid CB2 receptors in a mouse model of abeta amyloidosis: immunohistochemical analysis and suitability as a PET biomarker of neuroinflammation. *PLoS ONE* **10**, e0129618.

Shoemaker J. L., Seely K. A., Reed R. L., Crow J. P. and Prather P. L. (2007) The CB2 cannabinoid agonist AM-1241 prolongs survival in a transgenic mouse model of amyotrophic lateral sclerosis when initiated at symptom onset. *J. Neurochem.* **101**, 87–98.

Showalter V. M., Compton D. R., Martin B. R. and Abood M. E. (1996) Evaluation of binding in a transfected cell line expressing a peripheral cannabinoid receptor (CB2): identification of cannabinoid receptor subtype selective ligands. *J. Pharmacol. Exp. Ther.* **278**, 989–999.

Slavik R., Grether U., Muller Herde A. *et al.* (2015a) Discovery of a high affinity and selective pyridine analog as a potential positron emission tomography imaging agent for cannabinoid type 2 receptor. *J. Med. Chem.* **58**, 4266–4277.

Slavik R., Herde A. M., Bieri D., Weber M., Schibli R., Kramer S. D., Ametamey S. M. and Mu L. (2015b) Synthesis, radiolabeling and evaluation of novel 4-oxo-quinoline derivatives as PET tracers for imaging cannabinoid type 2 receptor. *Eur. J. Med. Chem.* **92**, 554–564.

Solas M., Francis P. T., Franco R. and Ramirez M. J. (2013) CB2 receptor and amyloid pathology in frontal cortex of Alzheimer's disease patients. *Neurobiol. Aging* **34**, 805–808.

Turkheimer F. E., Rizzo G., Bloomfield P. S., Howes O., Zanotti-Fregonara P., Bertoldo A. and Veronese M. (2015) The methodology of TSPO imaging with positron emission tomography. *Biochem. Soc. Trans.* **43**, 586–592.

Turkman N., Shavrin A., Paolillo V. *et al.* (2012) Synthesis and preliminary evaluation of [(18)F]-labeled 2-oxoquinoline derivatives for PET imaging of cannabinoid CB(2) receptor. *Nucl. Med. Biol.* **39**, 593–600.

Valenzano K. J., Tafesse L., Lee G. *et al.* (2005) Pharmacological and pharmacokinetic characterization of the cannabinoid receptor 2 agonist, GW405833, utilizing rodent models of acute and chronic pain, anxiety, ataxia and catalepsy. *Neuropharmacology* **48**, 658–672.

Van Camp N., Boisgard R., Kuhnast B. *et al.* (2010) In vivo imaging of neuroinflammation: a comparative study between [(18)F]PBR111, [(11)C]CLINME and [(11)C]PK11195 in an acute rodent model. *Eur. J. Nucl. Med. Mol. Imaging* **37**, 962–972.

Vandeputte C., Evens N., Toelen J. *et al.* (2011) A PET brain reporter gene system based on type 2 cannabinoid receptors. *J. Nucl. Med.* **52**, 1102–1109.

Vicidomini C., Panico M., Greco A. *et al.* (2015) In vivo imaging and characterization of [(18)F]DPA-714, a potential new TSPO ligand, in mouse brain and peripheral tissues using small-animal PET. *Nucl. Med. Biol.* **42**, 309–316.

Volkow N. D., Compton W. M. and Weiss S. R. (2014) Adverse health effects of marijuana use. *N. Engl. J. Med.* **371**, 879.

Wright K., Rooney N., Feeney M., Tate J., Robertson D., Welham M. and Ward S. (2005) Differential expression of cannabinoid receptors in the human colon: cannabinoids promote epithelial wound healing. *Gastroenterology* **129**, 437–453.

 